

KAPL-3158
AEC Research and
Development Report

KNOLLS
ATOMIC POWER
LABORATORY

AMPTIAC

Walt

3/8/68

this may be helpful

Joe Guffanti

DISTRIBUTION STATEMENT A
Approved for Public Release
Distribution Unlimited

(Fatigue Design Data
for the
Titanium Alloy, Ti-6Al-6V-2Sn)

72244

RETURN REPORTS
REGISTER FILE
IMMEDIATELY AFTER USE

20060516247

D.F. Mowbray

May 20, 1966

Operated for the
United States Atomic
Energy Commission by
GENERAL ELECTRIC

~~DOCUMENT LIBRARY COPY~~

~~DO NOT DESTROY~~

UNCLASSIFIED

KAPL-3158

UC-25, Metals, Ceramics, and
Materials
(TID-4500, 49th Edition)

FATIGUE DESIGN DATA FOR THE TITANIUM ALLOY, Ti-6Al-6V-2Sn

D. F. Mowbray

May 20, 1966

DISTRIBUTION STATEMENT A
Approved for Public Release
Distribution Unlimited

E. E. Baldwin

Authorized Classifier

Sept. 23, 1966

Date

General Electric Company
KNOLLS ATOMIC POWER LABORATORY
Schenectady, New York
Operated for the
United States Atomic Energy Commission
Contract No. W-31-109 Eng-52

UNCLASSIFIED

UNCLASSIFIED

LEGAL NOTICE

This report was prepared as an account of Government-sponsored work. Neither the United States, nor the Commission, nor any person acting on behalf of the Commission:

- A. Makes any warranty or representation, expressed or implied, with respect to the accuracy, completeness, or usefulness of the information contained in this report, or that the use of any information, apparatus, method, or process disclosed in this report may not infringe privately owned rights; or
- B. Assumes any liabilities with respect to the use of, or for damages resulting from the use of any information, apparatus, method, or process disclosed in this report.

As used in the above, "person acting on behalf of the Commission" includes any employee or contractor of the Commission, or employee of such contractor, to the extent that such employee or contractor of the Commission, or employee of such contractor prepares, disseminates, or provides access to, any information pursuant to his employment or contract with the Commission, or his employment with such contractor.

Printed in USA. Price \$2.00. Available from the Clearinghouse for Federal Scientific and Technical Information, National Bureau of Standards, U. S. Department of Commerce, Springfield, Virginia 22151.

UNCLASSIFIED

KAPL-3158

UNCLASSIFIED

KAPL-3158

UC-25, Metals, Ceramics, and
Materials

(TID-4500, 49th Edition)

(Nonstandard)

DISTRIBUTION

	<u>No. of Copies</u>
AEC, SNR	
Cramer, CC	3
Baldwin, EE	2
Division of Technical Information Extension	3
Document Library	4
Jekkals, I	1
Ferril, D	1
Glasser, TH	1
Kelleman, RW	1
Miles, A	1
McCalley, RB	1
Mehringner, FJ	1
Miller, DR	1
Mowbray, DF	5
Naval Reactors Library	2
Shriver, PR	1
Sokol, GJ	1
Technical Publications/JG Shaw	1
TIG File/CJ Schmidt	5
Total	<u>35</u>

UNCLASSIFIED

CONTENTS

	<u>Page</u>
ABSTRACT	ix
NOMENCLATURE	xi
INTRODUCTION	1
TEST DESCRIPTION	1
Material	1
Specimens	2
Test Equipment and Procedure	5
TEST RESULTS	6
DISCUSSION OF TEST RESULTS	10
Unnotched Fatigue Strength	10
Effect of Mean Stress on Unnotched Fatigue Strength	14
Notch Sensitivity	17
SUMMARY AND CONCLUSIONS	18
REFERENCES	19
APPENDIX A. MAXIMUM EFFECT OF MEAN STRESS BASED ON A PARABOLIC DAMAGE LAW	21
APPENDIX B. EQUATIONS FOR USE WITH THE δ -CONCEPT	23

ILLUSTRATIONS

<u>No.</u>	<u>Title</u>	<u>Page</u>
1	(0002) Pole Figure for the α -Phase of Rolled 1.0-in.-diam Bar (KS-62295, Unclassified)	3
2	Unnotched Cylindrical Fatigue Specimen (KS-62296, Unclassified)	3
3	Notched Cylindrical Fatigue Specimens (KS-62297, Unclassified)	4
4	Monotonic and Cyclic Stress-Strain Response at Room Temperature and at 600F (KS-62298, Unclassified)	7
5	Unnotched Fatigue Data (KS-62299, Unclassified)	8
6	Notched Fatigue Data (KS-62300, Unclassified)	12
7	Variation of Notch-Sensitivity Factor (q) with Notch-Root Radius (R) (KS-62301, Unclassified)	13
8	Comparison of Titanium Strain-Cycled Fatigue Strength with Other Materials (KS-62302, Unclassified)	14
9	Fatigue Damage Laws for Considering Mean Stress (KS-62303, Unclassified)	16

ABSTRACT

An investigation was conducted to determine some of the basic fatigue properties of the titanium base alloy (Ti-6Al-6V-2Sn) in the annealed bar stock form. The basic S-N curves in the cyclic life region from approximately 10^2 to 10^6 cycles, the effect of mean stress at lives from 10^4 to 10^6 cycles, and the effect of notches on fatigue strength at 10^6 cycles were established at room temperature and at 600F. P 2 →

The test results indicate that this material possesses good unnotched fatigue strength, but has a rather high sensitivity to mean stress and notches. These latter results are as expected because of the material's high ratio of yield to ultimate tensile strength.

The test results were analyzed in terms of current design methods. It was found that the effect of mean stress on the unnotched fatigue strength is best described by a parabolic damage law. Values of δ are established for estimating fatigue notch factors for members containing crack-like defects.

NOMENCLATURE

A	Minimum cross-sectional area of fatigue specimens, in. ²
δ	Distance from surface of notch root (see Reference 10), in.
D	Minimum section diameter of notched fatigue specimens, in.
ε _R	Cyclic strain range in unnotched fatigue tests, %
E	Young's modulus, psi
γ	Poisson's ratio (0.3 is assumed)
K	Ratio of local tensile stress to nominal net-section stress (σ/σ_n)
K _f	Fatigue-notch factor for axial load* (defined as the ratio of fatigue strength of unnotched specimen to fatigue strength of notched specimen at a given number of cycles to failure)
K _t	Theoretical elastic stress concentration factor for normal stress (σ_{max}/σ_n)
K' _t	Combined theoretical elastic stress concentration factor taking into account normal stress concentration factor and Mises criterion of failure (see Reference 2)
K _f ^δ	Fatigue-notch factor predicted by the δ-concept
K _{tn} ^δ	Theoretical elastic stress concentration factor at a distance δ from the notch-root surface for the normal stress in a notched cylindrical specimen
K _{tt} ^δ	Theoretical elastic stress concentration factor at a distance δ from the notch-root surface for the tangential stress in a notched cylindrical specimen
q	Fatigue-notch sensitivity factor, $\frac{K_f - 1}{K'_t - 1}$
R	Notch-root radius, in.
σ	Local tensile stress, psi
σ _{max}	Maximum elastically calculated tensile stress at notch root, psi
σ _n	Average net-section stress at the minimum section of a notched bar, psi

*Used in this report only for axial load.

- S_a Completely reversed (zero mean stress) stress amplitude* that produces failure in a given number of cycles ($E \times \epsilon_R/2$), psi
- S'_a Stress amplitude* that, combined with the maximum possible mean stress, produces failure in the same number of cycles as a completely reversed stress amplitude S_a , psi
- S_b Limit of elastic behavior, psi
- S_m Mean stress, $S_b - S'_a$, psi
- S_u Ultimate tensile strength, psi
- T Notch depth, in.
- Y Coordinate (see Figure B.1), in.

*Fictitious stress.

FATIGUE DESIGN DATA FOR THE TITANIUM ALLOY, Ti-6Al-6V-2Sn

D. F. Mowbray

INTRODUCTION

The application of high-strength titanium alloy, Ti-6Al-6V-2Sn, is being increased in the nuclear industry where fatigue loadings are commonly encountered in the low- and intermediate-cyclic-life regions over the range of temperature from 75 to 600F. To assist in the design of components fabricated from bar stock of this alloy, an investigation was undertaken to determine some of the basic fatigue properties at the cyclic lives and temperatures of interest. Displacement-controlled tests were conducted on unnotched specimens to establish fatigue curves and the so called "maximum effect of mean stress" over the cyclic life region of $\sim 10^2$ to 10^6 cycles; load-controlled tests were conducted on notched specimens to determine fatigue notch factors for several different geometries at 10^5 cycles. An equal number of tests were conducted at both 75 and 600F.

TEST DESCRIPTION

Material

The material used in this investigation was the titanium base alloy designated Ti-6Al-6V-2Sn.¹ This titanium alloy is double-vacuum-melted by consumable electrode techniques. The material was obtained as 1.0-in.-diameter hot-rolled bar stock in the fully annealed condition. The annealing treatment consisted of heating in vacuum at 1300F for 2-1/4 hr, followed by an air cool.

The chemical composition was as follows:

<u>Element</u>	<u>wt %</u>
Aluminum	5.6
Vanadium	5.5
Tin	2.0
Iron	0.76
Copper	0.71
Oxygen	0.155
Carbon	0.023
Nitrogen	0.018
Hydrogen	0.0053
Titanium	Remainder

The conventional tensile properties (in the rolling direction) at room temperature and at 600F are given in Table 1. Note the high-yield-to-ultimate-tensile-strength ratio exhibited by this material.

TABLE 1. CONVENTIONAL TENSILE PROPERTIES OF TEST MATERIAL*

Temperature, F	UTS, psi	0.2% YS, psi	0.2% YS UTS	Elongation in 2 in., %	RA, %
75	159,000	155,000	0.98	18.5	35.0
75	161,100	151,000	0.94	18.5	36.2
600	127,000	105,200	0.83	19.5	50.0
600	128,000	104,500	0.82	18.5	50.8

*The tensile and fatigue specimens were vacuum-annealed for 2 hr at 1300F following machining.

UTS Ultimate tensile strength
 YS Yield strength
 RA Reduction in area

In light of the fact that preferred orientations are known to develop in rolled titanium products, \sqrt{a} (0002) pole figure was determined for the α -phase (HCP structure) of the material used in this investigation. The pole figure, shown in Figure 1, indicates a very definite, preferred orientation with a preponderance of basal planes perpendicular to the rolling (and loading) axis.

Specimens

Axial specimens with their longitudinal axes in the rolling direction were used for both the unnotched and the notched tests. The unnotched specimen, shown in Figure 2, had a 0.160-in. diameter and was subjected to a constant-displacement cycle. Notched specimens incorporating 60-deg V-grooves were tested with two minimum-section diameters: 0.160 and 0.480 in. These specimens are shown in A and B, respectively of Figure 3. The 0.160-in. minimum-section-diameter specimens were tested with a single notch-root radius (0.001 in.). However, the 0.480-in. minimum-section diameter specimens were tested with notch-root radii of 0.0015, 0.005, and 0.015-in. It was originally intended that the larger diameter specimens be tested with a notch-root radius of 0.001-in. the same as the smaller diameter specimens, but a 0.0015-in.-notch-root radius was the smallest that could be achieved. All the notched specimens were subjected to a constant-load cycle.

P18

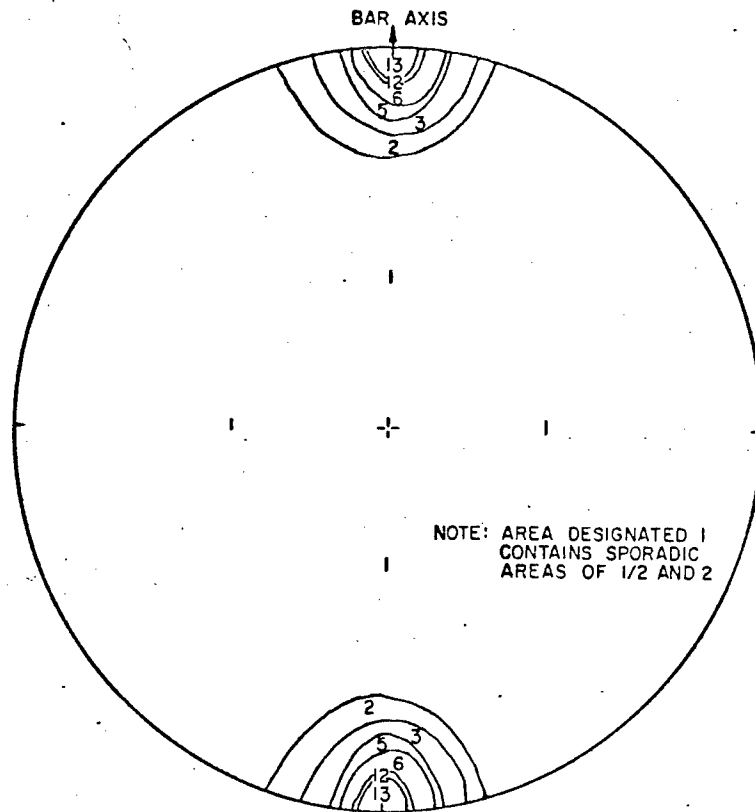
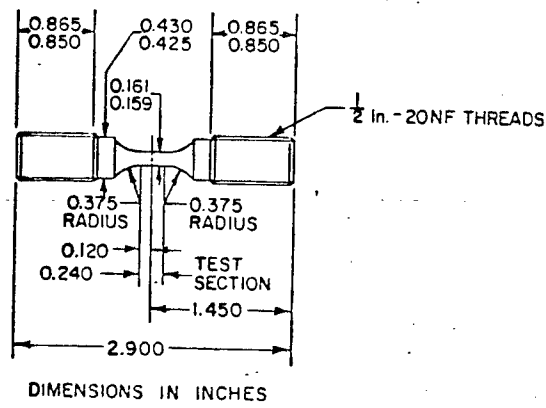


FIGURE 1. (0002) Pole Figure for the α -Phase of Rolled, 1.0-in.-diam Bar.

KS-62295

Unclassified

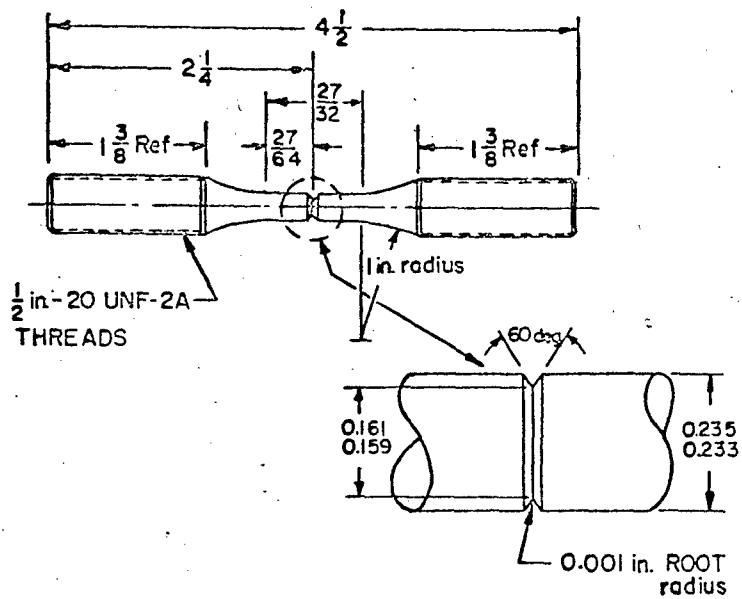


DIMENSIONS IN INCHES

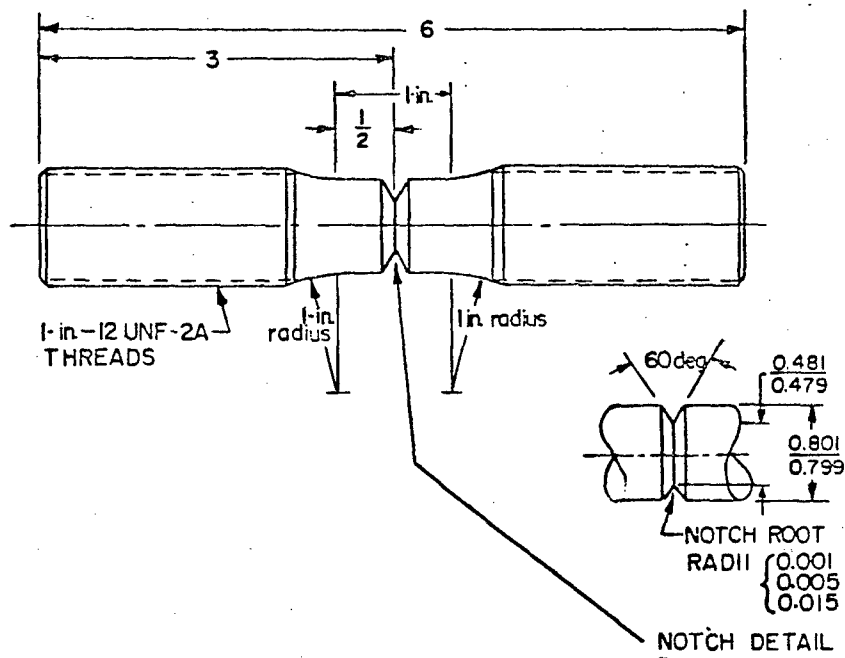
FIGURE 2. Unnotched Cylindrical Fatigue Specimen.

KS-62296

Unclassified



A. Small Diameter.



B. Large Diameter.

(All Dimensions in Inches)

FIGURE 3. Notched Cylindrical Fatigue Specimens.
KS-62297 Unclassified

All specimens were machined from the fully annealed bar stock. The machining was performed carefully to prevent excessive residual stresses on the specimen surface. After machining, the test-section surfaces of the unnotched specimens were polished with 600-grit paper in the longitudinal direction. The grooves in the notched specimens were finish-machined by a lapping operation which minimized the presence of machining scratches transverse to the test direction. Following final machining, the specimens were given an additional 2-hr vacuum-anneal at 1300F (vacuum was maintained at 10^{-5} mm Hg).

Test Equipment and Procedure

The test work in this investigation was conducted by Lessells and Associates, Inc., Waltham, Mass. The description of the test equipment and procedure to follow is abstracted from their data report.

The displacement-controlled tests were conducted in a test machine which has a rigid frame containing the specimen grips, the lower grip being driven by a rotating eccentric which may be set for any desired displacement amplitude. The upper specimen grip consists of a cylindrical rod threaded at its lower end to accept the specimen. It is free to slide vertically within a hole in the upper frame, except when clamped by screws on the split, upper crossbar of the frame. The lower grip slides in the lower crossbar of the frame, being guided by a very close fit with a cylindrical impregnated bearing which is pressed into the cross member. Attached to the bottom of the lower grip is a flex plate, below which is a push bar instrumented with strain gages for load measurement. The machine cycling rate is variable from 18 to 600 cpm. A cycling rate of 120 cpm was used for the tests at the lower strain amplitudes and a rate of 18 cpm at the higher strain amplitudes.

Specimen strain was measured by one of several methods. In tests conducted at room temperature at strains <1.9% range, strain gages were attached directly to the specimen test sections. Values of strain reported for these tests were the first-cycle strain-gage readings (i.e., no variation of strain range was noted during the tests). In four tests conducted at each of the two test temperatures at strains $\geq 4.0\%$ range, strain was measured by means of a diameter transducer gage, incorporating an LVDT. Values of strain reported for these tests are transducer readings at shakedown (the first cycle at room temperature and approximately the 100th cycle at 600F). This diameter-transducer gage was also used to measure strain in the remaining 600F tests (<1.5% range), but the gage was not considered by the author to yield sufficiently accurate measures of the strain. Consequently, the 600F strains reported at <1.5% range were determined by dividing the P/A stress by the elastic modulus. In all of these tests, the material appeared to remain elastic.

Signals from the load transducer, specimen strain gages, and diameter transducer were amplified and recorded on a Honeywell Visicorder. Records were made during the first twenty cycles and periodically thereafter.

A small split-shell resistance furnace with appropriate thermocouples and an indicating pyrometer-controller were used for the elevated-temperature tests. At 600F, the temperature gradient along the specimen test section was $<5F$.

The load-controlled tests were conducted on a Schenk six-ton vertical fatigue machine. This machine incorporates automatic control of the alternating load, and the temperature in a three-zone furnace when testing at elevated temperatures. At the 600F operating level, temperature level and test-section temperature gradient were within $\pm 2F$.

The purpose of the notched tests was to evaluate K_f only at 10^6 cycles. To accomplish this, six to nine specimens of each notch geometry were tested at each of the two test temperatures. Attempts were made in testing each group of specimens to fail some of the specimens below 10^6 cycles, some above 10^6 cycles, and some as near 10^6 cycles as possible. Values of K_f were then evaluated by plotting the six data points on σ_n vs cycles-to-failure coordinates, joining a mean line through the points, determining the value of σ_n corresponding to the mean line at 10^6 cycles, and dividing the unnotched value of S_a at 10^6 cycles by σ_n at 10^6 cycles. Specimen failure was considered to be complete specimen separation.

Use of a displacement-controlled unnotched test result and a load-controlled notched test result for determining K_f is justified in this case by virtue of the fact that the fatigue stresses at 10^6 cycles to failure were strictly elastic. This can be observed in Figure 4 where the cyclic and monotonic (static) stress-strain response at the two test temperature are plotted. The values of elastic moduli used for constructing the elastic portions of the curves were 15.0×10^6 psi at room temperature and 13.6×10^6 psi at 600F. These values are in agreement with dynamic test results obtained for the test material, dynamic values reported in Reference 1, and static stress and strain measurements made on the unnotched fatigue specimens at room temperature.

TEST RESULTS

The results of the room temperature and 600F unnotched fatigue tests are listed in Table 2, and plotted in A and B of Figure 5 in terms of fictitious stress amplitude ($E\epsilon_a/2$) and cycles to failure. Part A of Figure 5 presents the room temperature data and B of Figure 5 the corresponding data at 600F. Best-fit curves have been faired (by eye) through the data points for the fully-reversed cycle tests (zero pre-strain) to establish S-N curves over the range of cycles from $\sim 10^2$ to 10^6 .

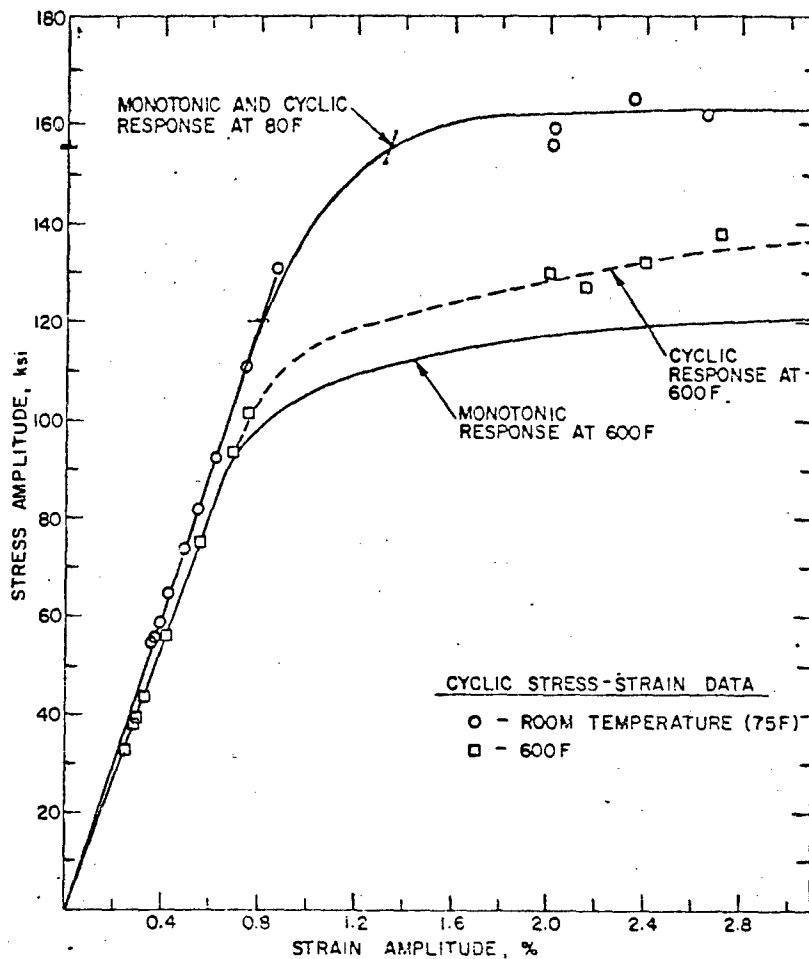


FIGURE 4. Monotonic and Cyclic Stress-Strain Response at Room Temperature and at 600F.
KS-62298

Unclassified

Data points for tests in which a 1.0% prestrain was superimposed are plotted in A and B of Figure 5 as solid points. The effect of the tensile prestrain is to reduce the cyclic strain required for failure in a given number of cycles at lives $>5 \times 10^3$. These reductions can be considered appreciable, particularly at room temperature. For materials like the present one, which possess high ratios of yield-to-ultimate tensile strength, this result should be anticipated.

In Table 2, the results discussed above are also reported in terms of strain range, which was the controlled test variable. Values of elastic moduli used for converting strain-range to fictitious stress-amplitude are those quoted in the previous section.

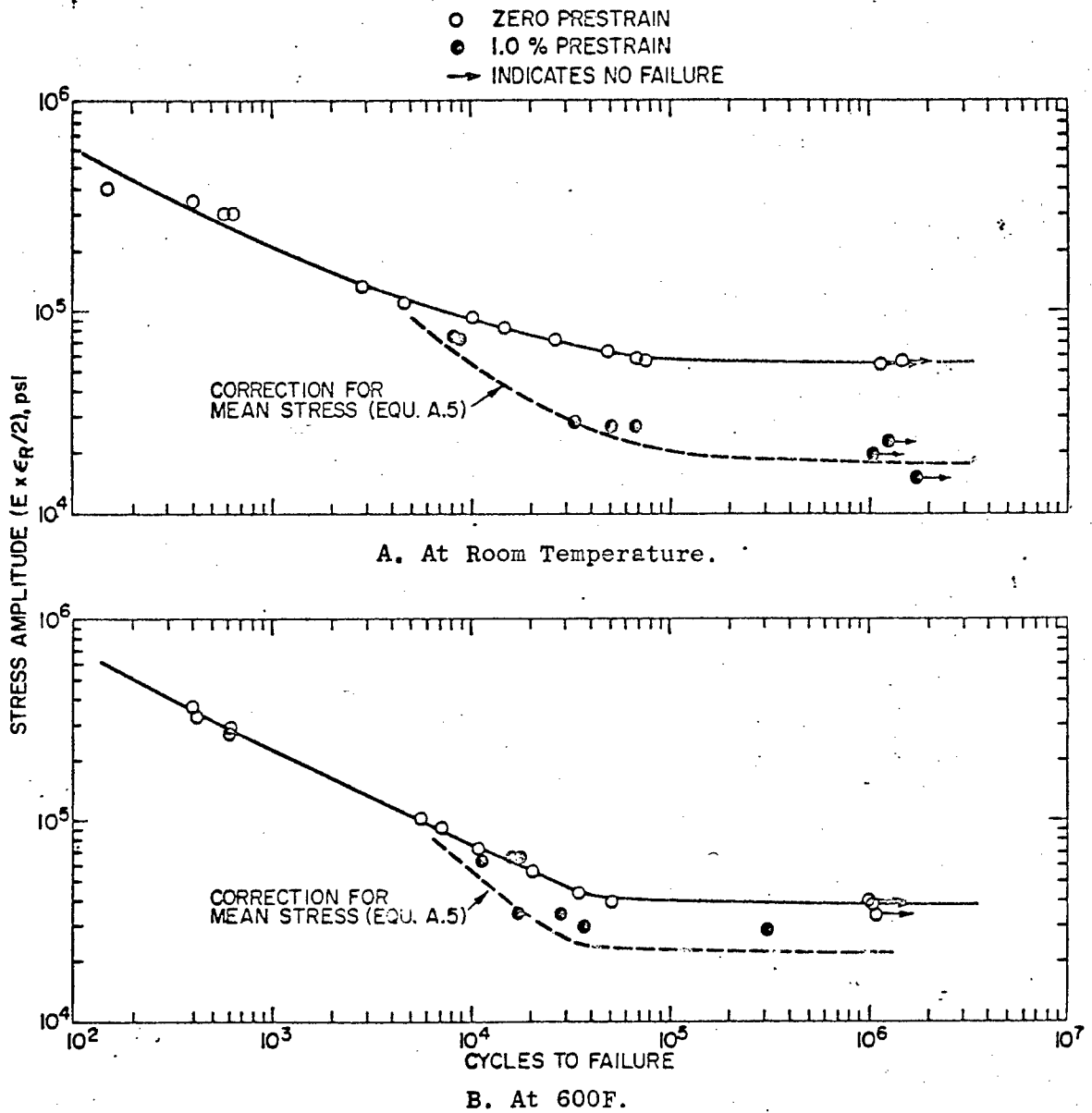


FIGURE 5. Unnotched Fatigue Data.
KS-62299 Unclassified

TABLE 2. UNNOTCHED FATIGUE TEST RESULTS

Test Temperature, F	Alternating Strain Range, %	Alternating Fictitious Stress Amplitude, psi	Prestrain, %	Cycles to Failure $\times 10^{-3}$	Failure	
75	5.30	397,000	0	0.151	-	
	4.70	352,000		0.400	-	
	4.08	306,000		0.573	-	
	4.04	303,000		0.619	-	
	1.75	131,000		2.82	-	
	1.47	110,000		4.57	-	
	1.23	92,500		10.4	-	
	1.09	81,800		14.7	-	
	0.98	73,500		26.8	-	
	0.85	63,000		58.0	-	
	0.78	58,500		78.0	-	
	0.78	58,500		85.5	-	
	0.75	56,200		1420.0	None	
	0.72	54,000		1110.0	None	
	1.00	75,000		1.0	8.37	-
	0.99	74,200		1.0	8.69	-
	0.38	28,500		1.0	33.3	-
0.36	27,000	1.0	66.9	-		
0.36	27,000	1.0	50.8	-		
0.30	22,500	1.0	1240.0	None		
0.26	19,500	1.0	1030.0	None		
0.20	15,000	1.0	1710.0	None		
600	5.44	372,000	0	0.402	-	
	4.79	328,000		0.414	-	
	4.30	294,000		0.617	-	
	4.00	274,000		0.619	-	
	1.50	102,800		5.60	-	
	1.38	94,500		7.06	-	
	1.10	74,500		10.9	-	
	0.82	55,700		20.4	-	
	0.65	44,200		34.7	-	
	0.59	40,100		51.4	-	
	0.59	40,100		1000.0	None	
	0.57	39,100		1030.0	None	
	0.50	34,300		1060.0	None	
	0.96	65,700		1.0	16.3	-
	0.96	65,700		1.0	18.5	-
	0.94	64,400		1.0	11.4	-
	0.50	34,300		1.0	17.5	-
0.50	34,300	1.0	28.4	-		
0.44	30,100	1.0	36.9	-		
0.42	28,800	1.0	310.0	-		

*Conf. deleted
 - for
 instructions
 K. F. Mowbray
 11-14-66
 66-29-60*

The results of the notched specimen tests are listed in Table 3 and plotted in Parts A and B of Figure 6 in terms of stress amplitude and cycles to failure. Part A of Figure 6 includes the data at room temperature and B of Figure 6 the corresponding data at 600F. Best-fit curves have been faired (by eye) through the data points for each notch geometry.

The values of K_f at 10^6 cycles derived from the notched and unnotched tests are listed in Table 4. Also listed are values of the notch sensitivity factor² (q) defined as:

$$q = \frac{K_f - 1}{K'_t - 1}$$

This factor is a commonly used index for judging the notch sensitivity of materials in fatigue. It provides a scale of notch sensitivity that varies from $q = 0$, or no notch effect, to $q = 1$, or full theoretical effect. Plots of q vs R for room temperature and for 600F are shown in Figure 7.

Attention is directed again to the stress-strain diagrams plotted in Figure 4. Note that the cycling did not alter the stress-strain behavior at room temperature (i.e., no cyclic hardening or softening), whereas at 600F the cycling caused a slight hardening. All the cyclic stress-strain data points plotted are first-cycle values except for the four at 600F which show a deviation from the monotonic curve. The stress values for these points correspond to the 100th cycle, where the peak-load values generally occurred.

DISCUSSION OF TEST RESULTS

Unnotched Fatigue Strength

The unnotched fatigue test results indicate that this particular alloy of titanium possesses good unnotched fatigue strength in air relative to other materials, when evaluated on a strain range basis. This is illustrated in Figure 8, where the unnotched and zero mean strain test results have been plotted in terms of strain range and cycles to failure. Shown for comparison is a scatter band for test results obtained by Manson and Hirschberg³ on fourteen different materials, including steels, aluminums, titaniums, and high-temperature alloys. Their individual data points for the titanium alloy, Ti-6Al-4V, heat treated to obtain an ultimate strength of 179,000 psi, are also shown.

TABLE 3. NOTCHED FATIGUE TEST RESULTS

Test Temperature, F	Notch-Root Radius, in.	Minimum-Section Diameter, in.	Stress Amplitude, psi	Cycles to Failure $\times 10^{-3}$	Failures
75	0.001	0.160	20,000	165.0	-
			20,000	136.0	-
			17,000	261.0	-
			17,000	10,000.0	None
	0.001	0.160	17,000	1,550.0	-
			17,000	282.0	-
			30,000	25.3	-
			25,000	39.6	-
	0.0015	0.480	20,000	130.0	-
			18,000	113.0	-
			15,000	260.0	-
			10,000	932.0	-
	0.0015	0.480	10,000	529.6	-
			20,000	75.0	-
			15,000	192.0	-
			15,000	400.0	-
	0.005	0.480	15,000	1,510.0	-
			14,000	285.0	-
			13,000	8,140.0	None
			12,000	15,110.0	None
0.005	0.480	10,000	12,020.0	-	
		30,000	40.1	-	
		25,000	147.0	-	
		25,000	149.0	-	
0.015	0.480	22,500	13,000.0	None	
		22,500	343.6	-	
		20,000	21,960.0	None	
		15,000	9,320.0	None	
600	0.001	0.160	17,000	340.0	-
			17,000	313.0	-
			17,000	328.0	-
			17,000	7,540.0	None
	0.001	0.160	20,000	157.0	-
			20,000	104.0	-
			12,000	570.0	-
			10,000	527.0	-
	0.0015	0.480	10,000	551.0	-
			10,000	463.0	-
			9,000	579.0	-
			9,000	8,000.0	None
	0.0015	0.480	8,000	4,490.0	-
			15,000	81.0	-
			15,000	186.0	-
			12,000	241.0	-
	0.005	0.480	12,000	337.0	-
			12,000	822.0	-
			12,000	921.0	-
			12,000	8,220.0	None
0.015	0.480	22,500	85.3	-	
		22,500	89.5	-	
		20,000	149.0	-	
		20,000	2,320.0	-	
0.015	0.480	20,000	5,090.0	-	
		20,000	5,300.0	-	

*See for
with ref.
11-14-66
17A.F. Summary
12-29-66*

8

TABLE 4. FATIGUE NOTCH FACTORS AND NOTCH SENSITIVITY
AT 10^8 CYCLES

Temperature, F	Notch Radius, in.	Notch Diameter, in.	K_t'	K_f	K_f^δ	q'
75	0.001	0.160	6.9	3.3	3.4*	0.39
75	0.0015	0.480	10.0	6.1	5.9*	0.57
75	0.005	0.480	5.7	4.5	4.6*	0.74
75	0.015	0.480	3.4	2.6	3.2*	0.67
600	0.001	0.160	6.9	2.4	2.5**	0.24
600	0.0015	0.480	10.0	4.3	4.3**	0.37
600	0.005	0.480	5.7	3.5	3.9**	0.53
600	0.015	0.480	3.4	2.0	2.9**	0.42

* $\delta = 0.0006$ in.

** $\delta = 0.0012$ in.

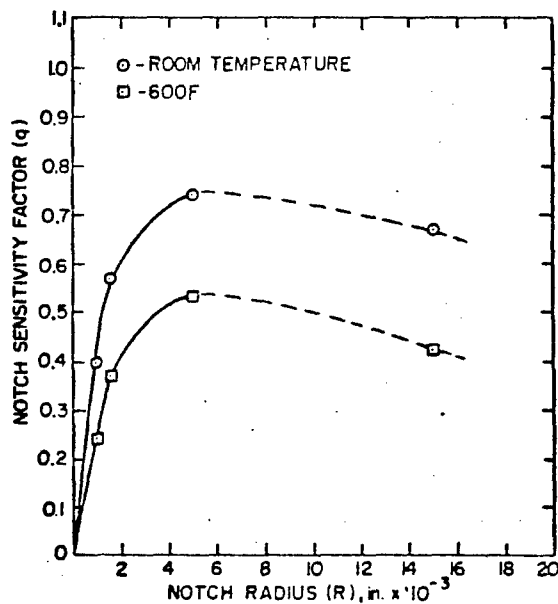


FIGURE 7. Variation of Notch-Sensitivity Factor (q) with Notch-Root Radius (R).

KS-62301

Unclassified

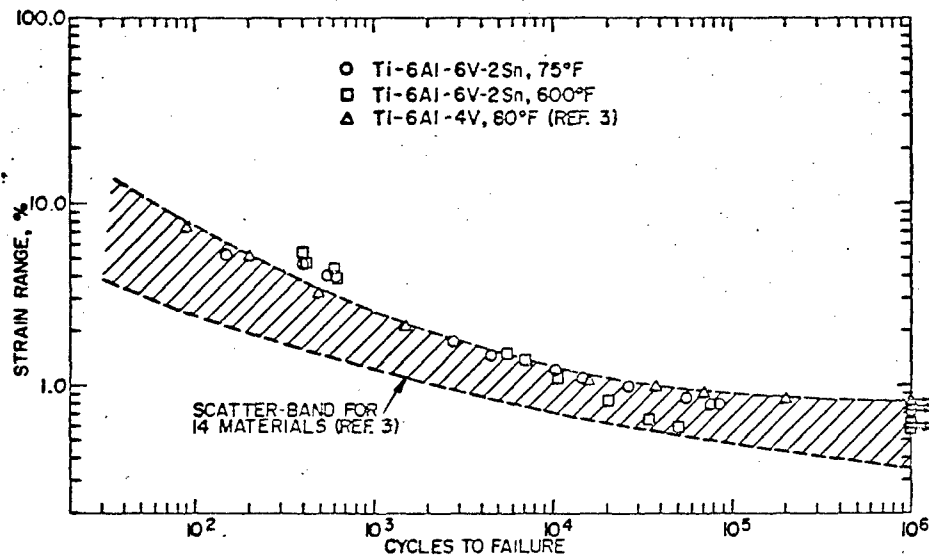


FIGURE 8. Comparison of Titanium Strain-Cycled Fatigue Strength with Other Materials.

KS-62302

Unclassified

The following observations are made:

1. The room temperature fatigue strength of the Ti-6Al-6V-2Sn alloy falls on the upper side of the scatter band, exceeding it in the low-cycle life region.
2. The 600F fatigue strength of the Ti-6Al-6V-2Sn alloy exceeds the scatter band in the low-cycle life region but falls to the lower side of the scatter band in the intermediate-cycle life region.
3. The room temperature fatigue strength of the Ti-6Al-4V alloy, heat-treated to obtain an ultimate tensile strength higher than that of the Ti-6Al-6V-2Sn alloy tested in this investigation (179,000 psi vs 160,000 psi), possesses slightly greater fatigue strength in the high-cycle life region but slightly less in the low-cycle life region.

Effect of Mean Stress on Unnotched Fatigue Strength

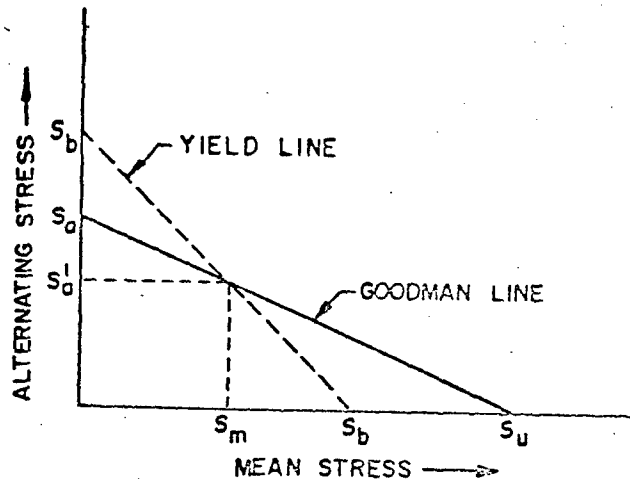
The effect of mean stress on the fatigue strength of the titanium alloy was studied by applying a prestrain of 1.0% to a number of the unnotched specimens. The static strain of 1.0% is small enough so that the damage imparted to the specimen and the effect observed on the properties can be considered to be due to mean stress.

Because of the large reductions in fatigue strength caused by the presence of mean stress, it was thought desirable, for design purposes, to describe the data by means of an empirical damage law. Two of the damage laws proposed for predicting the effect of mean stress on fatigue strength were examined in an attempt to describe the data; these were the Goodman (linear) and Gerber (parabolic) laws.⁴ These were employed in the form in which the Goodman law is presently used for establishing design curves for material being strain-cycled.^{5,6} The design procedure incorporates a method for estimating the maximum effect of mean stress on the fatigue strength. At present, this method is based on the following assumptions:

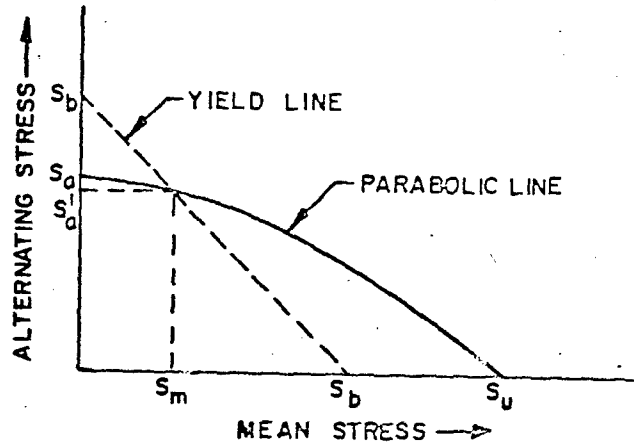
1. Plastic deformation will limit the maximum cyclic stress to the "limit of elastic behavior" (S_p).
2. Actual stress-strain behavior can be approximated by an elastic-perfectly plastic stress-strain curve, provided that the idealized value of yield stress is chosen sufficiently large.
3. A modified Goodman diagram (Part A of Figure 9) accounts for the fatigue damage due to mean stress.
4. The limit of elastic behavior (S_p) can be estimated by a 0.2% offset to the monotonic stress-strain curve or the cyclic stress amplitude-strain amplitude curve, if the material's stress-strain response is altered by cycling. The choice of a 0.2% offset strain is arbitrary.

To determine the maximum effect of mean stress, a yield line is superimposed on the modified Goodman diagram for each fatigue life (Part A of Figure 9); the largest mean stress that can be maintained at a given fatigue life corresponds to the intersection of the Goodman and yield lines. The fatigue curve is then adjusted for the maximum effect of mean stress.

The above method has been devised assuming idealized stress-strain behavior. For actual materials, which always exhibit some strain hardening, this method will be conservative, provided the strain corresponding to the selected value of S_p is \geq the maximum strains expected in service. For total strains exceeding the offset strains corresponding to S_p , the amount of mean stress that can be supported becomes a function of the strain hardening and maximum total strain, as well as the cyclic strain. Despite the fact that the above described method is not necessarily conservative for cases where the maximum strain exceeds the strain corresponding to S_p , as was the case in this investigation where a value of 1.0% mean strain was applied, it has previously been found that this method provides a suitable working theory for describing Zircaloy^{6,7} and Inconel⁸ test data.



A. Modified Goodman Diagram.



B. Gerber Parabolic Diagram.

FIGURE 9. Fatigue Damage Laws for
Considering Mean Stress.

KS-62303

Unclassified

Attempts to describe the titanium data with the Goodman law in the method for estimating the maximum effect of mean stress did not yield satisfactory results. The correction to the fatigue curve fell well below the experimental data. For this reason the Gerber law was employed with the same method to see if a better description of the data could be achieved. The results are shown in A and B of Figure 5 by the dotted lines. One can observe that the maximum effect of mean stress concept incorporating the Gerber parabolic damage law produces a fairly good description of the test data, although it appears conservative in the very high cyclic life region. Values of S_p and S_u used were 150,000 and 160,000 psi at room temperature and 120,000 and 130,000 psi at 600F. An equation expressing the maximum effect of mean stress in terms of the Gerber law is derived in Appendix A.

Notch Sensitivity

The high values of K_f (a maximum value of 5.9) determined by the fatigue tests and the steep rise in the q vs R curves of Figure 7, at the low values of R , indicate that this particular titanium alloy has a high fatigue-notch sensitivity. At notch radii ≤ 0.005 in., the room-temperature fatigue-notch sensitivity is comparable to that of heat-treated steel having a tensile strength of 200,000 psi;⁹ the 600F notch sensitivity is comparable to that of heat-treated steel having a tensile strength of 125,000 psi.⁹ There is, however, some relaxation in the high-notch sensitivity at the larger radii, as the values of q are less at $R = 0.015$ in. than at $R = 0.005$ in. For most materials, the q vs R curve does not achieve a maximum, but continues to rise with increasing R , asymptotically approaching a q value of 1.0.

Another method used for expressing the fatigue-notch sensitivity of metals is the δ -concept. The δ -concept is based on the premise that the stress at some finite distance, δ , below the notch root is the stress which limits fatigue life. The concept considers that because metals are granular structures and because fatigue cracks initiate on slip planes in the grains, it should be necessary to increase the elastic stress amplitude so that the fatigue limit below the notch root is exceeded to some finite depth, which is denoted δ . By considering a finite volume of material below the notch root, the δ -concept takes into consideration stress gradient effects. That is, it predicts that K_f increases as the net-section thickness increases, and that K_f is a maximum for some value of notch-root radius >0 .

The δ -concept is especially useful for estimating the fatigue-notch factors for crack-like defects. Experimental values of K_f are generally not available for crack-like defects for which $R \rightarrow 0$ and $K_t \rightarrow \infty$. A paper by O'Donnell and Purdy¹⁰ demonstrated the use of the δ -concept for

estimating fatigue-notch factors for cracks. In that paper, elastic notch-stress distributions were calculated by the method of Neuber¹¹ for notched flat bars in bending and tension. The procedure used for estimating K_f for a crack involves the plotting of K_f^δ (for a given section thickness) for a range of R and the selecting of the maximum value. The maximum occurs for a finite notch radius, usually in the range from 0.0005 to 0.002 in. Of course it must be kept in mind that the appropriate value of δ must be determined experimentally with finite notch-radii specimens.

Extension of the δ -concept for use with cylindrical bars, including the appropriate equations for stress distributions, is described in Appendix B. Values of δ determined from the experimental test results of this investigation are 0.0006 in. at room temperature and 0.0012 in. at 600F. Agreement between notch factors determined using these values of δ (K_f^δ) and the experimental values (K_f) can be observed in Columns 5 and 6 in Table 4. The values of δ quoted have been selected so that K_f^δ agrees with K_f at the smaller notch-root radii and yield conservative estimates of K_f for larger notch-root radii.

It should be noted that both of the above concepts for expressing fatigue-notch sensitivity are based on crack initiation as a failure criterion, and the data reported here are for fracture. The use of fracture data is justified on the basis that the major portion of fatigue life for failure in 10^6 cycles involves crack initiation. Nevertheless, the use of crack initiation data could possibly improve correlations of this type.

SUMMARY AND CONCLUSIONS

The following fatigue design properties have been established at room temperature and at 600F (in air) for the titanium base alloy, Ti-6Al-6V-2Sn, in the annealed bar stock form:

1. Strain-controlled fatigue curves covering the cyclic-life region from $\sim 10^2$ to 10^6 cycles.
2. The corrections to the fatigue curves for the "maximum effect of mean stress;" determined for applied prestrains of 1.0%.
3. Notch sensitivity for sharply notched cylindrical bars including factors for estimating K_f of crack-like defects.

The test results support the following conclusions about the fatigue properties of this material:

1. It possesses good, unnotched fatigue strength in air relative to other materials, when considered on a strain-range basis.
2. It has a high sensitivity to mean stress, particularly at room temperature.
3. It has a high sensitivity to sharp notches (<0.005 in. notch-root radius).

REFERENCES

1. Titanium Engineering Bulletin No. 10, "Properties of Ti-6Al-6V-2Sn," Titanium Metals Corporation of America.
2. Peterson, R. E. Stress Concentration Design Factors. New York: John Wiley and Sons, Inc. 1953.
3. Manson, S. S., and M. H. Hirschberg. "Fatigue Behavior in Strain Cycling in the Low- and Intermediate-Cycle Range." Fatigue - An Interdisciplinary Approach. Syracuse University Press. 1964. Pp. 133-173.
4. Richards, C. W. Engineering Materials Science. Wadsworth Publishing Company, Inc. Pp. 356-360.
5. Langer, B. F. "Design of Pressure Vessels for Low-Cycle Fatigue." J. of Basic Engr. 84, September 1962. P. 389.
6. O'Donnell, W. J., and B. F. Langer. "Fatigue Design Basis for Zircaloy Components." Nuc. Sci. and Eng. 20, 1964. Pp. 1-12.
7. Mowbray, D. F. "Effects of 1.0% Superimposed Mean Strain on the Bending Fatigue Strength of Zircaloy-4." Nuclear Applications, I. February 1, 1965. Pp. 39-48.
8. Mowbray, D. F., G. J. Sokol, and R. E. Savidge. "Fatigue Characteristics of Ni-Cr-Fe Alloys with Emphasis on Pressure Vessel Cladding." KAPL-3108. July 1, 1965.
9. Peterson, R. E. "Analytical Approach to Stress Concentration Effect of Aircraft Materials." WADC-TR-59-507. August 1959. Pp. 273-299.
10. O'Donnell, W. J., and C. M. Purdy. "The Fatigue Strength of Members Containing Cracks." ASME Trans. 86B2. May 1964. P. 205.
11. Neuber, H. "Theory of Notch Stresses: Principles for Exact Calculation of Strength with Reference to Structural Form and Material." AEC-TR-4547. 1961.

APPENDIX A. THE MAXIMUM EFFECT OF MEAN STRESS BASED
ON THE GERBER PARABOLIC DAMAGE RELATIONSHIP

The Gerber parabolic law for representing the effect of combined alternating and mean stress is⁴

$$\frac{S'_a}{S_a} + \left(\frac{S_m}{S_u}\right)^2 = 1 \quad (A.1)$$

To determine an expression for the so-called "maximum effect of mean stress," the point of intersection of the yield line and parabola defined by Equation A.1 must be located as shown in Part B of Figure 9, p. 16.

The equation of the yield line is

$$S'_a = S_b - S_m \quad (A.2)$$

Upon solving for S_m in Equations A.1 and A.2 and equating, the following relationship results:

$$\frac{S'_a}{S_a} + \frac{(S_b - S'_a)^2}{S_u^2} = 1 \quad (A.3)$$

Solving Equation A.3 for S'_a results in the following:

$$S'_a = \left(S_b - \frac{S_u^2}{2S_a}\right) + S_u \sqrt{\left(\frac{S_u^2}{4S_a^2} + 1\right)} - \frac{S_b}{S_a} \quad (A.4)$$

The criterion for evaluating the mean-stress correction to the S-N curve using the Gerber parabolic damage relationship is then

$$S'_a = \left(S_b - \frac{S_u^2}{2S_a}\right) + S_u \sqrt{\left(\frac{S_u^2}{4S_a^2} + 1\right)} - \frac{S_b}{S_a} \quad \text{for } S_a < S_b \quad (A.5)$$

$$S'_a = S_a \quad \text{for } S_a > S_b$$

APPENDIX B. EQUATIONS FOR USE WITH THE δ -CONCEPT

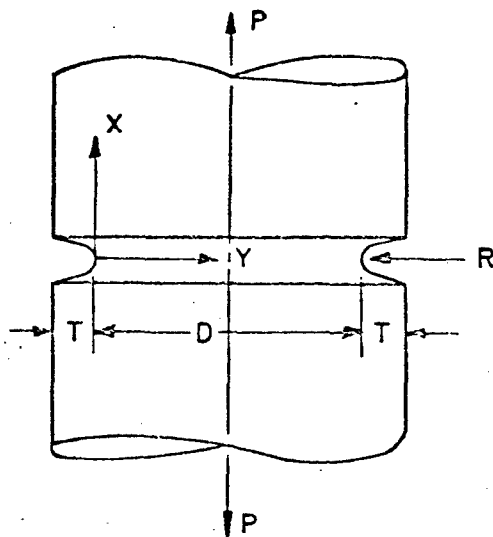
If the elastic stress distribution in the minimum section is expressed as (see Sketch B.1),

$$K = K(Y, R, D, T), \quad (B.1)$$

the fatigue-notch factor is defined according to the δ -concept as

$$K_f \equiv K(\delta, R, D, T) = K_f^\delta \quad (B.2)$$

δ is treated as a material property and must be determined by experiment.



Sketch B.1. Notched Cylindrical Bar.

The von Mises criterion of failure was used to take into consideration the multiaxial fatigue stresses in the vicinity of the notches. Considering the radial stress component as negligible, K_f can be expressed by the von Mises criterion as (considering fatigue rather than yielding):

$$K_f^\delta = \frac{1}{\sqrt{2}} \sqrt{\left(\bar{K}_{tn}^\delta - \bar{K}_{tt}^\delta\right)^2 + \left(\bar{K}_{tn}^\delta\right)^2 + \left(\bar{K}_{tt}^\delta\right)^2} \quad (B.3)$$

It is recognized that use of the von Mises criterion with this material is not strictly correct because of probable anisotropic behavior. However, in lieu of fatigue properties in more than one test direction, it is considered the best that is available.

The method of Neuber¹¹ was used to calculate the notch-stress distributions. Neuber has derived nearly exact solutions for infinitely wide members containing shallow and deep notches. For the intermediate region between shallow and deep notches, he suggests use of an interpolation formula. It should be noted that the notch-stress distributions are also based on isotropic theory. The appropriate equations for the normal and tangential stress distributions are given below:

1. Normal stress

$$\bar{K}_{tn} = 1 + \frac{(K_s - 1)(K_{tn} - 1)}{\sqrt{(K_s - 1)^2 + (K_{tn} - 1)^2}} \quad (B.4)$$

2. Tangential stress

$$\bar{K}_{tt} = 1 + \frac{K'_s K_{tt}}{\sqrt{(K'_s)^2 + K_{tt}^2}} \quad (B.5)$$

where

$$K_s = 1 + \frac{\cosh u_0}{2(\cosh^2 u + 1)} \left[e^{u_0} \left(e^{2u_0} - 3 \right) \left(1 + \frac{1}{2} \frac{\cosh u}{\sqrt{\cosh^2 u - 1}} \right) + \frac{\cosh u_0 \cosh u}{\sqrt{\cosh^2 u - 1}} \right] \quad (B.6)$$

$$\cosh u = \left(1 + \frac{Y}{T} \right) \cosh u_0 \quad (B.7)$$

$$\cosh u_0 = \sqrt{\frac{T/R}{T/R - 1}} \quad (B.8)$$

$$\sinh u_0 = \frac{1}{\sqrt{T/R - 1}} \quad (\text{B.9})$$

$$K'_s = v (K_s - 1) \quad (\text{B.10})$$

$$K_{tn} = \frac{1}{\sqrt{1 - \left[\left(1 - \frac{2Y}{D} \right) \sin v_0 \right]^2}} \left\{ C + 2E(-1 + v) \right\} \\ + \frac{1}{\left\{ 1 - \left[\left(1 - \frac{2Y}{D} \right) \sin v_0 \right]^2 \right\}^{3/2}} \left\{ -B + C \right\} \quad (\text{B.11})$$

$$K_{tt} = \frac{1}{\left\{ 1 - \left[\left(1 - \frac{2Y}{D} \right) \sin v_0 \right]^2 \right\}^{1/2}} \left\{ B \right. \\ \left. \times \frac{1}{1 + \sqrt{1 - \left[1 - \left(1 - \frac{2Y}{D} \right) \sin v_0 \right]^2}} - C - 2vE \right\} \quad (\text{B.12})$$

$$B = (1 - 2v)(1 + \cos v_0) E \quad (\text{B.13})$$

$$C = B - E \cos^2 v_0 \quad (\text{B.14})$$

$$E = -\frac{1}{2} \left[\frac{1 + \cos v_0}{1 + 2v \cos v_0 + \cos^2 v_0} \right] \quad (\text{B.15})$$

$$\sin v_0 = \sqrt{\frac{D/2R}{D/2R + 1}} \quad (\text{B.16})$$

$$\cos v_0 = \frac{1}{\sqrt{D/2R + 1}} \quad (\text{B.17})$$